Nuclear Inst. and Methods in Physics Research, A 898 (2018) 85–89

Contents lists available at ScienceDirect

Nuclear Inst. and Methods in Physics Research, A

journal homepage: www.elsevier.com/locate/nima

Neutron sensitivity of $^{10}B_4C$-coated aluminum honeycomb using a single-anode wire, P-10 continuous-gas-flow proportional counter

Nathaniel S. Edwards *, Kyle A. Nelson, Niklas J. Hinson, Christopher N. Tiner, Michael A. Reichenberger, Ryan G. Fronk, Douglas S. McGregor

S.M.A.R.T. Laboratory, Department of Mechanical and Nuclear Engineering, Kansas State University, Manhattan, KS 66505, USA

ARTICLE INFO

Keywords:
Neutron detection
Gas-filled radiation detector
Neutron converter
Thin-film-coated substrate
^{3}He alternative

ABSTRACT

The intrinsic thermal-neutron detection efficiency of a $^{10}B_4C$-coated aluminum honeycomb sample was measured using a single-anode wire, P-10 continuous-gas-flow proportional counter. The aluminum honeycomb sample was 1.27 cm thick with a diameter of 4.1275 cm (1 5/8 in.) and was composed of hexagonal-shaped cells with a cell size of 1.5875 mm (1/16 in.). The $^{10}B_4C$ coating was applied by Exothermics, Inc. via magnetron sputtering to a coating thickness of 4.68 ± 1.25 μm as measured using a scanning electron microscope. Using a lower level discriminator setting of 50 keV, intrinsic thermal-neutron detection efficiency was measured to be $21.45 \pm 0.26\%$ in reference to a 4.0 atm, 5.08-cm (2-in.) diameter, 15.24-cm (6-in.) long Reuter Stokes ^{3}He tube with a known efficiency of $80.7 \pm 0.5\%$. MCNP6 simulations yielded a theoretical intrinsic thermal-neutron detection efficiency of approximately 24% for a $^{10}B_4C$-coating thickness of 4.68 μm with a lower level discriminator setting of 50 keV.

1. Introduction

Several alternative neutron detection technologies have been developed to achieve the neutron detection and gamma-ray discrimination capabilities of commercially-available ^{3}He proportional counters at a fraction of the cost [1–5]. Given the abundant deployment of commercial ^{3}He proportional counters in the oil-well logging industry [6–8], motivation exists to define alternative neutron-conversion materials that are capable of operating in oil-well logging instrumentation temperatures up to 200 °C [9,10].

Honeycomb substrates have recently emerged as a substrate of interest for thin-film-coated thermal-neutron detection applications [11–15] due to the amount of surface area contained within a compact substrate size. Specifically, boron-lined honeycomb substrates have previously been fabricated and tested either with individual anode wires positioned within each individual honeycomb cell [12] or with a series of gas electron multipliers positioned below the substrate [13–15]. A representative picture of the substrate geometry is shown in Fig. 1. These light-weight substrates are commonly used in commercial industries as energy absorbers, structural materials, and directional flow guides due to their high strength-to-weight ratio [16]. Several companies manufacture these substrates [16–19] using various materials such as plastics and aluminum and the size and shape of the cells can be adjusted depending on the desired application [16,17,20]. The present work reports on the measurement and simulation of the intrinsic thermal-neutron detection efficiency, ε_{th}, of a $^{10}B_4C$-coated aluminum honeycomb sample tested using a single-anode wire, P-10 continuous-gas-flow proportional counter.

2. Theoretical considerations

Thin-film-coated devices are inherently limited to allowing only one reaction product to enter into the ionizing volume of the detector [22,23]. Given that a single layer of ^{10}B or ^{6}LiF thin-film-coating has a maximum ε_{th} of approximately 4.5% [23,24], several alternating converter-ionization volume layers are required to achieve the performance of commercially-available ^{3}He proportional counters [22,23]. A variety of approaches have been explored to implement consecutive thin-film coatings contained within various sizes and shapes of ionizing volumes in order to increase ε_{th} [12,15,25–28].

Depending on the size and geometry of the ionization volume, thin-film-coated devices commonly rely on either ^{10}B or ^{6}Li as the neutron-converting isotope. For smaller ionization volumes, ^{10}B (and ^{10}B-containing compounds such as $^{10}B_4C$ and ^{10}BN) is used due to its higher thermal-neutron absorption cross section (3840 b for ^{10}B compared to 940 b for ^{6}Li [22,23,29]) coupled with the shorter range of reaction

* Corresponding author.
E-mail address: nedwards@ksu.edu (N.S. Edwards).

https://doi.org/10.1016/j.nima.2018.04.046
Received 16 February 2018; Received in revised form 13 April 2018; Accepted 23 April 2018
Available online 2 May 2018

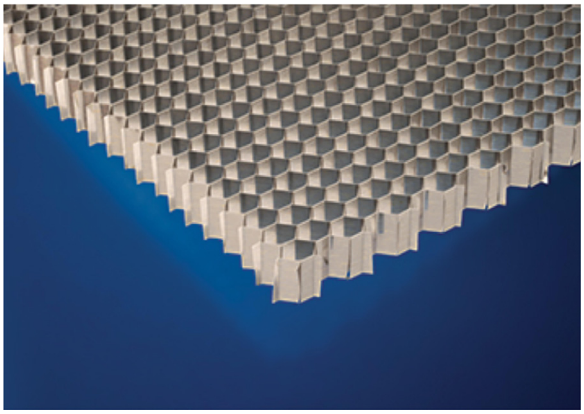

Fig. 1. Geometry of an aluminum honeycomb substrate [21]. The walls of the honeycomb substrate are coated with a thin layer of neutron-converting material for use as a compact, high-efficiency neutron counter.

products emitted from the $^{10}B(n,\alpha)\,^7Li$ reaction [22,23].$^{10}B_4C$ is commonly used as a thin-film-coating material instead of ^{10}B because of its desirable material and adhesion properties [30–33]. The addition of carbon results in a slight decrease of the macroscopic thermal-neutron absorption cross section of $^{10}B_4C$ compared to that of ^{10}B, reducing it to approximately 450 cm^{-1} from 500 cm^{-1} [34,35]. The density and melting temperature for $^{10}B_4C$ of 2.45 g cm^{-3} [36] and 2350 °C [37], respectively, are slightly higher than that of ^{10}B of 2.15 g cm^{-3} [35] and 2075 °C [37]. Thus,$^{10}B_4C$ was selected as the thin-film-coating material for the present work because it is capable of being deployed in high temperature environments with similar neutron-detection capabilities compared to pure-^{10}B.

When a neutron is absorbed by a ^{10}B atom, charged-particle reaction products are emitted in opposite directions with energies described by,

$$ {}^{1}_{0}n + {}^{10}_{5}B \rightarrow \begin{cases} {}^{7}_{3}Li\ (1.015\,\mathrm{MeV}) + {}^{4}_{2}He\ (1.777\,\mathrm{MeV}),\ 6\% \\ {}^{7}_{3}Li_{*}\ (0.840\,\mathrm{MeV}) + {}^{4}_{2}He\ (1.470\,\mathrm{MeV}),\ 94\% \end{cases}. \tag{1} $$

As shown in Eq. (1), the 6% and 94% reaction branches have reaction Q-values of 2.792 and 2.310 MeV, respectively. The discrepancy in reaction Q-values arises from the ^7Li ion of the 94% branch being emitted in its first excited state. A rapid de-excitation of the ^7Li ion to its ground state results in the emission of a 0.480 MeV gamma ray.

In general, three reaction-product emission scenarios exist for a thin-film-coated substrate, as illustrated in Fig. 2. In scenarios 1 and 2, one of the reaction products is able to escape the reactive layer and enter into the gas while the other reaction product is absorbed within the coating and/or substrate. Once inside the gas, liberation of charge carriers occurs as the reaction product ionizes the gas. Charge induction occurs as the charge carriers drift toward their respective electrodes under the influence of an electric field formed by the potential difference between the electrodes. In scenario 3, both charge carriers are absorbed within the reactive coating and/or substrate and thus cannot be measured. Although three scenarios are shown in Fig. 2, the amount of energy deposited by the reaction-product within the gas depends on the emission site and trajectory of the reaction product. As a result, reaction-product pulse-height spectra measured using a thin-film-coated device typically have a distribution of deposited energies represented, ranging up to the full energy of the highest-energy reaction product [38].

3. Experimental methods

A 1.27-cm (0.5-in.) thick, 4.1275-cm (1.625-in.) diameter aluminum-honeycomb sample containing hexagonal cells with a cell size of 1.5875 cm (1/16 in.) was coated with $^{10}B_4C$ via magnetron sputtering by Exothermics, Inc. Fig. 3 illustrates the honeycomb cell parameters relative to the coating thickness. The $^{10}B_4C$ coating thickness was measured to be 4.68 ± 1.25 μm using a Hitachi S-3400N scanning electron microscope. Twenty-four sample locations were measured in order to establish a distribution of coating thicknesses about the entire sample. Shown in Fig. 4 are representative measurements of the $^{10}B_4C$-coating thickness.

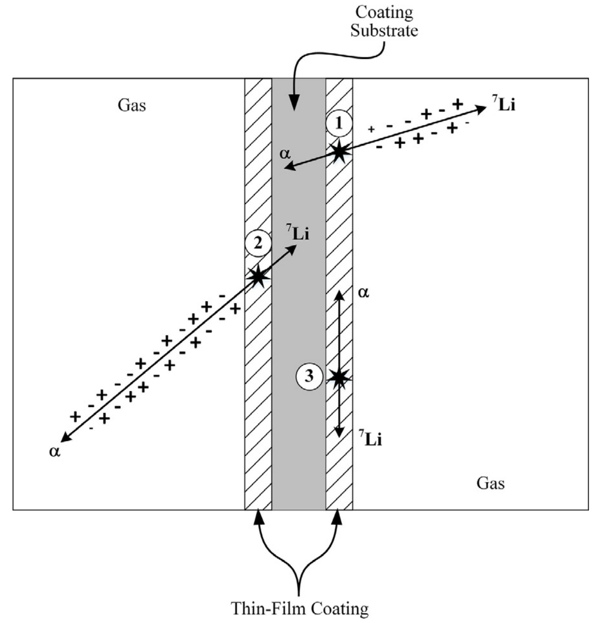

Fig. 2. General reaction-product emission scenarios that occur from neutron conversion using a thin-film-coated device.

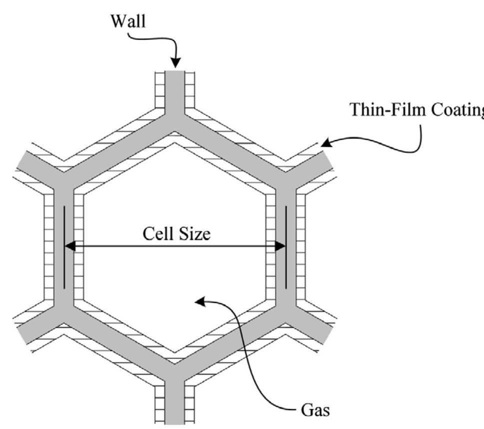

Fig. 3. Top-down illustration of the honeycomb cell and coating parameters. The honeycomb material is represented in gray, the thin-film coating in horizontal cross-hatching, and the gas in white.

The sample was then positioned within a continuous-gas-flow proportional counter containing a 25.4-μm diameter tungsten anode wire, as illustrated in Fig. 5. The continuous-gas-flow proportional counter was connected to a tank of P-10 proportional gas (90% argon, 10% methane). Measurement of ε_{th} was conducted using the diffracted neutron beam of the Kansas State University TRIGA Mk II research reactor. The test apparatus was positioned to align the side of the sample with the incident thermal-neutron beam as illustrated in Fig. 5. A cadmium collimator with a 5-mm diameter aperture was used to ensure the thermal-neutron beam was incident strictly on the side of the sample, eliminating solid-angle effects. The $^{10}B_4C$-coated aluminum-honeycomb sample ε_{th} was calculated in reference to a 4.0 atm, 5.08-cm (2-in.)

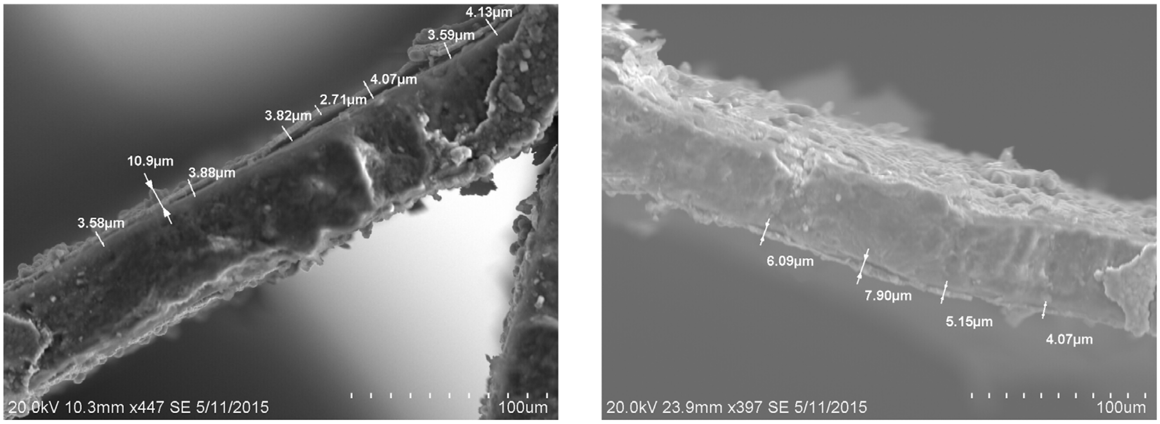

Fig. 4. $^{10}B_4C$-coating thicknesses measured using a scanning electron microscope. Several locations were measured about the sample in order to obtain an average $^{10}B_4C$-coating thickness distribution.

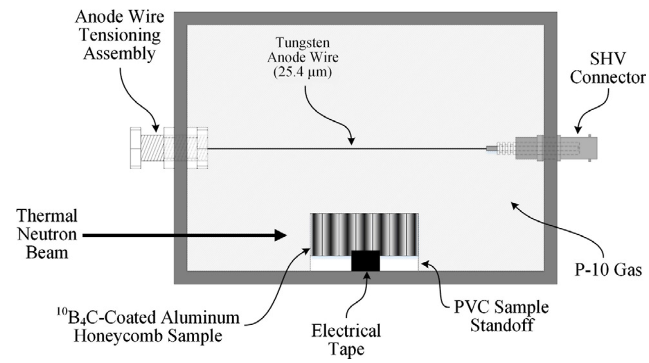

Fig. 5. A cross-sectional view of the thermal-neutron beam orientation relative to the $^{10}B_4C$-coated aluminum honeycomb sample positioned within the single-anode wire, continuous-gas-flow proportional counter testing device. P-10 gas continuously flowed through the chamber during the ε_{th} and energy-calibration measurements.

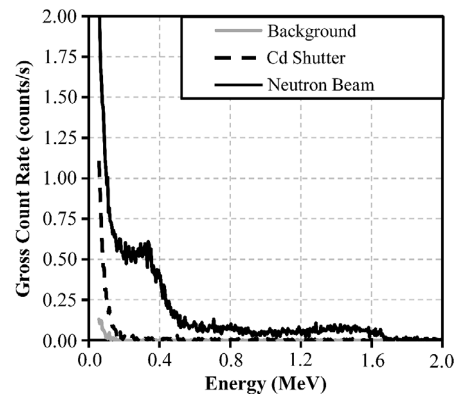

Fig. 6. Measured reaction-product pulse-height spectrum of the $^{10}B_4C$-coated aluminum honeycomb sample relative to a background measurement and a measurement in which the cadmium shutter blocked the incident thermal-neutron beam. The LLD setting was calculated to be 50 keV.

diameter, 15.24-cm (6-in.) long Reuter Stokes ^{3}He tube with a known ε_{th} of 80.7 ± 0.5% [39,40]. The continuous-gas-flow proportional counter was operated with the anode wire maintained at an experimentally-determined operating voltage of 700 V. Energy calibration of the measured reaction-product spectrum was accomplished using a ^{148}Gd alpha-particle source that was positioned within the continuous-gas-flow proportional counter once ε_{th} testing concluded.

MCNP6 simulations were performed for the distribution of measured $^{10}B_4C$-coating thicknesses applied to the aluminum honeycomb sample. The simulation environment included a 5-mm diameter beam of thermal neutrons incident on the center of the side of the sample. P-10 proportional gas at ambient pressure was implemented into the simulation environment in an attempt to accurately match the experimental environment. Uniform $^{10}B_4C$-coating thicknesses of 3.5–6.0 µm were simulated to compare to the measured average coating thickness and associated error (4.68 ±1.25 µm).

4. Results and discussion

The resulting reaction-product pulse-height spectra measured for the cases of reactor off (i.e. background), reactor on with Cd neutron shutter closed, and reactor on with Cd neutron shutter open are shown in Fig. 6. The experimental ε_{th} was calculated to be 21.45 ± 0.26% for a lower level discriminator (LLD) setting of 50 keV in reference to the energy-calibration measurement.

The distributions of simulated ε_{th} as a function of $^{10}B_4C$-coating thickness for various LLD settings ranging from 0 to 100 keV are shown in Fig. 7. For a 50 keV LLD setting, the simulated ε_{th} varies from approximately 33%–19% for $^{10}B_4C$-coating thicknesses ranging from 3.5–6.0 µm, respectively. A comparison of the measured and simulated ε_{th} reveals that the measured ε_{th} occurs within the range of simulated values for similar LLD settings. Upon closer inspection, the simulated ε_{th} for a $^{10}B_4C$-coating thickness of 4.68 µm, the average coating thickness measured from the sample, was approximately 24% with a LLD setting of 50 keV. The difference between measured and simulated ε_{th} at the average coating thickness indicates that the measured coating thickness does not represent the true average coating thickness of the sample. Specifically, the measured coating thickness was a representation of several locations measured on the exterior surfaces of the sample. Given that magnetron sputtering was the coating method, which is a line-of-sight coating method, a broader distribution of coating thicknesses is likely present about the entirety of the sample, for both internally- and externally-located coating surfaces.

5. Conclusions

An aluminum honeycomb substrate coated with 4.68 ± 1.25µm of $^{10}B_4C$ had a measured ε_{th} of 21.45 ± 0.26% with an LLD setting of 50 keV. The measured ε_{th} occurred within the range of MCNP6-simulated values for $^{10}B_4C$-coating thicknesses ranging from 3.5 –6.0 µm. Specifically, the simulated ε_{th} was approximately 24% for a coating thickness

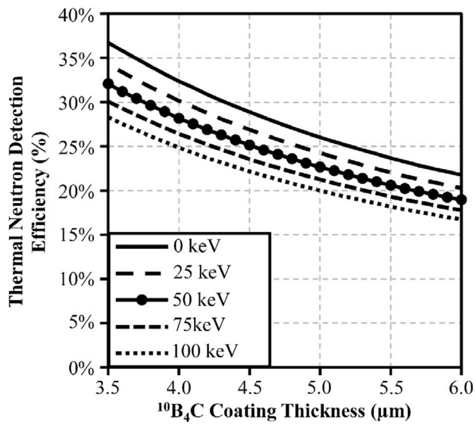

Fig. 7. MCNP6-simulated ε_{th} as a function of $^{10}B_4C$-coating thickness ranging from 3.5–6.0 μm for various LLD settings. As the LLD setting is increased for a given coating thickness, ε_{th} decreases.

of 4.68 μm with an LLD setting of 50 keV. Although the reason for the difference between measured and simulated values is unknown at the average coating thickness of 4.68 μm, it is suspected to be a function of the measured coating-thickness distribution as well as potentially the LLD setting.

Future efforts to improve the accuracy of the measured coating thickness require an increased number of positions about the sample to be measured for both internally- and externally-located coating surfaces. The number of measurements conducted should also be increased to improve the statistical accuracy of the measured average coating thickness. Finally, additional energy-calibration measurements using multiple and different known alpha-particle energies are necessary to clarify the energy-specific LLD setting used while measuring ε_{th}.

Although the measured and simulated efficiencies are significantly lower than commercially-available ^{3}He proportional counters, the results indicate that the substrate has the potential to be a viable candidate for a ^{3}He alternative technology. However, further experimental and simulation efforts are necessary to optimize the neutron-detection performance of the substrate as a thin-film-coated neutron-conversion medium.

Acknowledgments

This work was supported in part by the U.S. Defense Threat Reduction Agency (DTRA), under contract HDTRA1-12-c-0002.$^{10}B_4C$ coatings were applied via magnetron sputtering by Exothermics, Inc. MCNP6 simulations and experiment preparation efforts were performed at the Kansas State University Semiconductor Materials and Radiological Technologies (S.M.A.R.T.) Laboratory (Manhattan, KS). The authors wish to express their gratitude to the Kansas State University TRIGA Mk II research reactor staff for their assistance during neutron sensitivity testing.

References

[1] R.T. Kouzes, The ^{3} He Supply Problem, Pacific Northwest National Laboratory, Richland, WA, 2009.
[2] D.A. Shea, D. Morgan, The Helium-3 Shortage: Supply, Demand, and Options for Congress, in: CRS Reports for Congress, 2010.
[3] R.T. Kouzes, J.H. Ely, L.E. Erikson, et al., Neutron detection alternatives to ^{3}He for national security appliications, Nucl. Instrum. Methods A 623 (3) (2010) 1035–1045.
[4] A.J. Hurd, R.T. Kouzes, Why new neutron detector materials must replace helium-3, Eur. Phys. J. Plus 129 (10) (2014) 1–3.
[5] R.T. Kouzes, A.T. Lintereur, E.R. Siciliano, Progress in alternative neutron detection to address the helium-3 shortage, Nucl. Instrum. Methods A 784 (2015) 172–175.
[6] Schlumberger, Imaging density neutron standoff caliper service, https://www.slb.com/media/Files/drilling/product_sheets/lwd/pathfinder_lwd/idnsc_ps.pdf?la=en&hash=C31B3584DCFA98AF11D4818BE2132ACD8A451A1E. [September 1, 2017].
[7] Schlumberger, HPHT slim density, neutron, standoff, caliper tool, https://www.slb.com/media/Files/drilling/product_sheets/lwd/pathfinder_lwd/survivor_sdnsc_density_neutron_ps.pdf?la=en&hash=64DE2BD7A299C74B04A29268C5FB9C8EB0861DAB. [September 1, 2017].
[8] H.E. Services, Halliburton Logging and Perforating Capabilities for High-Pressure, High-Temperature Wells and Slim Holes, Halliburton Energy Services, Houston, 1995.
[9] A. Nikitin, S. Bliven, Needs of well logging industry in new nuclear detectors, in: IEEE Nuclear Science Symposuim & Medical Imaging Conference, Knoxville, TN, 2010, pp. 214-1219, Oct. 30–Nov. 6.
[10] Saint-Gobain Ceramics & Plastics Inc, Standard Geophysical Detectors, http://www.crystals.saint-gobain.com/sites/imdf.crystals.com/files/documents/standard-geophysical-detectors_69792.pdf, [February 15, 2017].
[11] K.A. Nelson, An Investigation of Aerogels, Foams, and Foils for Multi-Wire Proportional Counter Neutron Detectors, Doctorate, Mechanical and Nuclear Engineering, Kansas State University, 2013.
[12] Y. Yang, C. Li, C. Chen, et al. Research of boron lined honey-comb neutron detector realized with atomic layer deposition, in: 2013 IEEE Nuclear Science Symposium and Medical Imaging Conference, 2013 NSS/MIC, pp. paper N7-1, 3 pages, Oct. 27 - Nov. 2, 2013.
[13] Z. Fang, Y. Yang, Y. Li, The research of high detection efficiency boron lined detector with a honeycomb neutron converter, 2015 IEEE Nuclear Science Symposium and Medical Imaging Conference, NSS/MIC, 2015, paper N5A3-3, 4 pages, Oct. 31 - Nov. 7.
[14] Z. Fang, Y. Yang, Y. Li, et al., Working gas selection of the honeycomb converter-based neutron detector, IEEE Trans. Nucl. Sci. 64 (7) (2017) 1683–1688.
[15] Z. Fang, Y. Yang, Y. Li, et al., Research on a neutron detector with a boron-lined honeycomb neutron converter, IEEE Trans. Nucl. Sci. 64 (4) (2017) 1048–1055.
[16] Plascore, Honeycomb Cores. https://www.plascore.com/download/datasheets/honeycomb_data_sheets/Plascore_Honeycomb_LineCard.pdf. [August 31, 2017].
[17] Alcore, Commercial Grade Honeycomb, https://www.thegillcorp.com/alcore/datasheets/CGH.pdf, [August 31, 2017].
[18] Cel Components, Honeycombs and foams for sandwich panels. http://www.honeycombpanels.eu/14/honeycombs-and-foams-for-sandwich-panels, [August 31, 2017].
[19] Core Composites, Aluminum Honeycomb. http://www.corecomposites.com/products/honeycom/aluminum-honeycomb.html, [August 31, 2017].
[20] Plascore, Honeycomb Selector Guide. https://www.plascore.com/download/datasheets/honeycomb_data_sheets/Plascore_Selector.pdf, [August 31, 2017].
[21] Plascore, PAMG-XR1 5052 Aluminum Honeycomb. https://www.plascore.com/honeycomb/honeycomb-cores/aluminum/pamg-xr1-5052-aluminum-honeycomb/, [August 31, 2017].
[22] G.F. Knoll, Radiation Detection and Measurement, fourth ed., John Wiley & Sons Inc., Hoboken, NJ, 2010.
[23] D.S. McGregor, M.D. Hammig, Y.H. Yang, et al., Design considerations for thin film coated semiconductor thermal neutron detectors—I: basics regarding alpha particle emitting neutron reactive films, Nucl. Instrum. Methods A 500 (1–3) (2003) 272–308.
[24] D.S. McGregor, S.L. Bellinger, J.K. Shultis, Present status of microstructured semiconductor neutron detectors, J. Cryst. Growth 379 (2013) 99–110.
[25] D.S. McGregor, S.L. Bellinger, R.G. Fronk, et al., Development of compact high efficiency microstructured semiconductor neutron detectors, Radiat. Phys. Chem. 116 (2015) 32–37.
[26] Z. Wang, C.L. Morris, Multi-layer boron thin-film detectors for neutrons, Nucl. Instrum. Methods A 652 (1) (2011) 323–325.
[27] J.L. Lacy, A. Athanasiades, L. Sun, et al., Boron-coated straws as a replacement for ^{3}He-based neutron detectors, Nucl. Instrum. Methods A 652 (1) (2011) 359–363.
[28] J. Birch, J.C. Buffet, J. Correa, et al., $^{10}B_4C$ multi-grid as an alternative to ^{3}He for large area neutron detectors, IEEE Trans. Nucl. Sci. 60 (2) (2013) 871–878.
[29] N. Tsoulfanidis, Measurement and Detection of Radiation, second ed., Taylor & Francis, Washington, DC, 1995.
[30] C. Höglund, J. Birch, K. Andersen, et al., B_4C thin films for neutron detection, J. Appl . Phys. 111 (10) (2012) 104908.
[31] F. Piscitelli, Novel boron-10-based detectors for neutron scattering science, Eur. Phys. J. Plus 130 (2) (2015) 1–9.
[32] F. Piscitelli, P.V. Esch, Analytical modeling of thin film neutron converters and its application to thermal neutron gas detectors, J. Instrum. 8 (04) (2013) P04020.
[33] D.S. McGregor, R.T. Klann, H.K. Gersch, et al., New surface morphology for low stress thin-film-coated thermal neutron detectors, IEEE Trans. Nucl. Sci. 49 (4) (2002) 1999–2004.
[34] N.S. Edwards, K.A. Nelson, C.N. Tiner, et al. Charge propagation through- and neutron sensitivity of- reticulated vitreous carbon foam, in: 2015 IEEE Nuclear Science Symposium and Medical Imaging Conference, NSS/MIC, San Diego, CA, pp. paper N5A3-5, 4 pages, Oct. 31–Nov. 7, 2015.

[35] J.K. Shultis, D.S. McGregor, Design and performance considerations for perforated semiconductor thermal-neutron detectors, Nucl. Instrum. Methods A 606 (3) (2009) 608–636.
[36] C. Höglund, K. Zeitelhack, P. Kudejova, et al., Stability of $^{10}B_4C$ thin films under neutron radiation, Radiat. Phys. Chem. 113 (2015) 14–19.
[37] W.M. Hayes, D.R. Lide, CRC Handbook of Chemistry and Physics: A Ready-Reference Book of Chemical and Physical Data, CRC Press, Boca Raton, FL, 2007.
[38] D.S. McGregor, J. Kenneth Shultis, Spectral identification of thin-film-coated and solid-form semiconductor neutron detectors, Nucl. Instrum. Methods A 517 (1–3) (2004) 180–188.
[39] D.S. McGregor, W.J. McNeil, S.L. Bellinger, et al., Microstructured semiconductor neutron detectors, Nucl. Instrum. Methods A 608 (1) (2009) 125–131.
[40] D.S. McGregor, J. Kenneth Shultis, Reporting detection efficiency for semiconductor neutron detectors: a need for a standard, Nucl. Instrum. Methods A 632 (1) (2011) 167–174.